S. G. MOGILNY [1], *Professor, Doctor of Engineering Sciences*
A. A. SHOLOMITSKII [2], *Professor, Doctor of Engineering Sciences*
N. S. KOSAREV [2, 3], *Associate Professor, PhD, kosarevnsk@yandex.ru*
V. V. KAZANTSEVA [2, 3], *Senior Lecturer*
D. S. OZHIGIN [3], *Associate Professor, PhD*
S. B. KULIBABA [4], *Leading Researcher, Doctor of Engineering Sciences*

[1] *DonNTU, Donetsk, Russia*
[2] *SSUGiT, Novosibirsk, Russia*
[3] *Abylkas Saginov Karaganda Technical University, Karaganda, Kazakhstan*
[4] *Academician Melnikov Research Institute of Comprehensive Exploration of Mineral Resources–IPKON, Russian Academy of Sciences, Moscow, Russia*

ACCURACY ASSESSMENT OF AERIAL PHOTOGRAMMETRY FOR EMBANKMENT DAM MONITORING*

The article presents an overview of contemporary methods for monitoring deformations of embankment dams and dikes, including geodetic monitoring techniques and remote sensing methods such as terrestrial and aerial laser scanning and unmanned aerial vehicle (UAV) photogrammetry. A detailed analysis of the Sherubai-Nura Reservoir dam UAV image processing was conducted. The analysis showed that the coordinates of approximately 50% of the points in the object model were obtained by machine vision (MV) methods from only two images. A statistical relationship was identified between the number of images in which a point appears and the root mean square errors of point coordinates in the object model. Based on the analysis, recommendations for improving the accuracy of determining point coordinates in the model were formulated. It is shown that to achieve an accuracy of 0.05 meters, a point must be recognized in at least 9 images. Research has shown that increasing the number of images per point should not be achieved by increasing overlap between images and flight lines, as this does not improve photogrammetric intersection angles. Instead, mutually perpendicular flight lines and flight lines with an oblique camera orientation should be used. An important factor for point recognition in images by MV algorithms is the ground sampling distance (GSD) which should not exceed 2 cm/pixel. The authors note that self-calibration of images should be applied with caution unless appropriate conditions are met. In any case, it is advisable to use camera calibration on special high-precision calibration targets. By applying these recommendations, periodic monitoring of embankment dam deformations can be performed with high accuracy, thereby improving the operational safety of the structures.

Keywords: *UAV, RMS, monitoring, dykes, dams, aerial photogrammetry, digital camera, machine vision algorithms, deformations*
DOI: *10.17580/em.2026.01.10*

Introduction

Monitoring of embankment structures, which include dams and dykes of power plants, tailings storage facilities and protective hydraulic structures, is a necessary condition for their safe operation. Methods for monitoring such structures in the Russian Federation and in the Republic of Kazakhstan are regulated by normative-technical documentation (NTD) [1–4]. Among foreign NTD, special attention should be given to a document that provides recommendations for geotechnical monitoring, including the use of geodetic methods [5]. It is worth noting that no single normative-technical document covers all aspects of monitoring, especially for embankment structures.

Geodetic monitoring methods [6] allow determination of structural deformations with high accuracy; however, they require installation of permanent control points within a dam body and are labor-intensive. Geodetic monitoring typically determines surface settlements or displacement vectors at discrete points of the structures, which are most often located only along the dam crest. Therefore, this type of monitoring is inherently point-based.

For monitoring embankment dams, it is preferable to conduct areal measurements rather than point-based ones, covering the entire monitored structure. The analysis of multi-temporal surveys allows assessment of object deformations throughout the entire observation cycle. The most suitable methods for areal monitoring are laser scanning and LiDAR surveying. Terrestrial laser scanning) allows achieving the required monitoring accuracy [7]; however, it is not applicable in all cases and cannot be considered a tool for real-time monitoring. LiDAR surveying has significant potential for application in areal monitoring; however, in terms of the cost-to-quality ratio, it currently lags behind terrestrial laser scanning. Therefore, at present, aerial photography using unmanned aerial vehicles (UAVs) is actively used for areal monitoring of various engineering structures, including embankment structures [8–10].

The analysis of research results published by authors [11–15] shows that the accuracy of deformation determination from aerial photography materials with subsequent post-processing is about 5 cm. This level of accuracy is sufficient for seasonal deformation assessments of the structure during periods when the water level is at its highest and vegetation minimally obstructs survey data processing.

In this article, the authors describe their experience in conducting UAV-based aerial photography of the earth-fill dam of the Sherubai-Nura Reservoir, and analyze the influence of survey and camera parameters on the accuracy of determining point coordinates in the 3D model.

Monitoring object and UAV aerial survey technology

The object of study is the dam (embankment) of the Sherubai-Nura Reservoir in the Karaganda Region of the Republic of Kazakhstan. The dam was commissioned in 1960 and has been in operation for over 60 years. In terms of the structural type, the facility is an earth-fill dam. Long-term operation subjects the structure to seasonal temperature cycles, freeze–thaw actions, wind and water erosion, as well as changes in the water level regime in the reservoir. These factors collectively create conditions conducive to the development of deformation processes,

*The authors express their gratitude to Valeria Vyacheslavovna Dedkova, PhD, Associate Professor of the Department of Photogrammetry and Remote Sensing at the Siberian State University of Geosystems and Technologies, for her valuable comments and suggestions, which improved the content of this article.

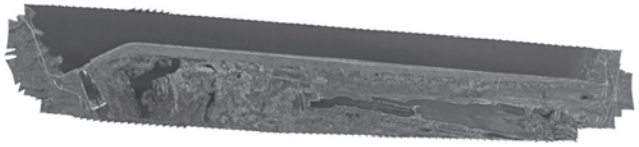

Fig. 1. Orthophoto map (orthomap) of the dam

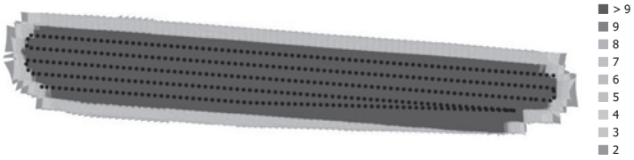

Fig. 2. Photograph centers and image overlap (survey of May 2025)

necessitating the application of modern methods for monitoring the structure geometry and stability.

Areal monitoring of the dam was carried out through two multi-temporal observation series (in May and September 2025) using a DJI Mavic 3 Enterprise. The survey was conducted according to a planned grid flight pattern ensuring 80% forward overlap and 70% side overlap. This provided sufficient measurement redundancy for generating an orthophoto map (**Fig. 1**) and a digital surface model, as well as for subsequent comparison of the multi-temporal models.

In both aerial survey series, the same UAV imaging system—DJI M3E camera—was used. According to the metadata of the source images, the survey was conducted with the following parameters: aperture f/2.8, shutter speed 1/1000 s, sensitivity ISO 180, focal length 12 mm (equivalent to 24 mm), and average metering mode. These camera parameters and exposure conditions ensured stable image characteristics and eliminated the influence of changes in imaging equipment on the comparability of results between the May and September series. The differences between the series were primarily determined by changes in flight altitude and resolution, while maintaining constant overlap of 80/70% (**Table 1**).

Figure 2 shows a diagram with photograph centers and image overlap. According to this diagram, most survey points should appear in more than 9 images.

Accuracy of model point coordinates

The geometric and computational meaning of the indicators characterizing the accuracy of the data on the position of points on the dam surface can be explained in a simplified form using **Fig. 3**.

An aerial photograph is considered a central projection of the terrain onto a plane, assuming that the real image has been corrected using the camera self-calibration method [16, 17]. Computer vision has identified points $a_1,\ldots a_5$ on the photographs as images of the same terrain point. Straight lines $a_1S_1,\ldots,a_5S_5$, originating from the image points on the photos and passing through the optical centers of the camera lens, form projection rays during the reconstruction of 3D model points from the set of photographs. Since the elements of exterior orientation and the central projection model contain random errors, the projection rays do not intersect at a single point on the model surface but intersect it at points $a'_1,\ldots a'_5$. Therefore, the coordinates of a point ρ are calculated

Table 1. Survey parameters

Date of survey	Number of images	Number of flight lines	Number of points	Flight altitude, m	GSD, cm/pixel
05.2025	407	5	711 109	200	5.23
09.2025	870	7	1 541 444	124	3.19

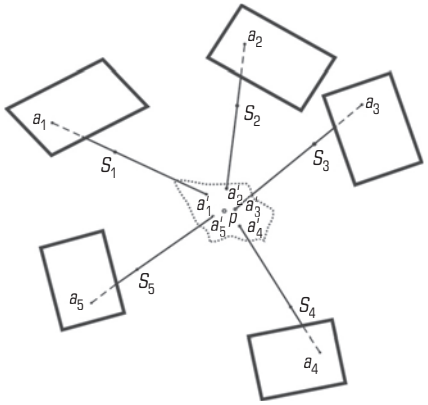

Fig. 3. Schematic of calculating terrain point coordinates from aerial photographs

such that the set of distances from p to points $a'_1,\ldots a'_5$ is, in a certain sense, minimized. It is assumed that the point ρ lies on the model surface, and its coordinates are equal to the coordinates of the corresponding terrain point. The projection rays form an uncertainty region around the point ρ, within which the true position of the terrain point a lies. The dimensions of this region are referred to as the accuracy of the coordinates of the terrain point. Since the positions of the projection rays depend on the random errors in the data used, the measure of accuracy is the covariance matrix of the point ρ, computed during the adjustment of the photogrammetric network by the least squares method using the bundles of projection rays.

In generalized form, the computation algorithm can be described as follows: collinearity equations are formed for the projection rays. In their linearized form, for a point i in an image j, these equations are described by the following expression.

$$\left.\begin{array}{l} A_{ij}\delta_{X_i} + B_{ij}\Delta + l_{ij} = v_{ij} \\ (i = 1, 2, \ldots, t;\ j = 1, 2, \ldots, s) \end{array}\right\}, \quad (1)$$

where A_{ij} is the design matrix in front of the correction vector δ_{X_i} to the geodetic coordinates X_i of the ground point i; B_{ij} is the design matrix in front of the correction vector Δ to the estimated network parameters; l_{ij} is the vector of constant terms; v_{ij} is the correction vector to the measured image coordinates of the point.

The system of equations (1) is solved simultaneously by the least squares method (LSM) under the condition that:

$$[p_v vv] = \min, \quad (2)$$

where p_v is the weight of the coordinates of corresponding points in the image.

In accordance with the theory of the LSM, formulas (1) and (2) correspond to the normal equations:

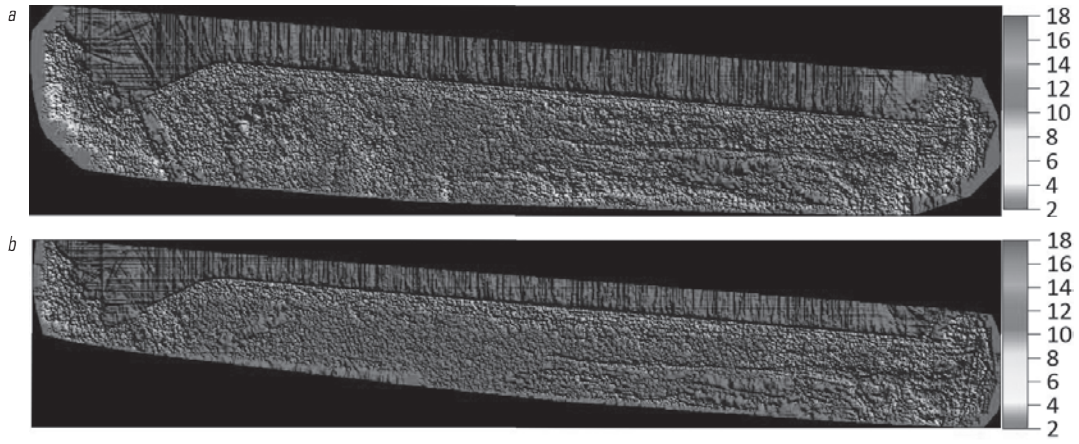

Fig. 4. Distribution of number of images used to determine coordinates of each object point:
a – Survey of May 2025 ; *b* – Survey of September 2025

$$\begin{bmatrix} C_{ii} & C_{i\Delta} \\ C_{i\Delta}^T & N_{\Delta\Delta} \end{bmatrix} \begin{bmatrix} \delta_{X_i} \\ \Delta \end{bmatrix} + \begin{bmatrix} L_{\delta_{Xi}} \\ L_\Delta \end{bmatrix} = 0, \quad (3)$$

where C_{ii} is the coefficient submatrix corresponding to the corrections δ_{X_i} to the coordinates X_i of ground point i; $N_{\Delta\Delta}$, $C_{i\Delta}$ are the submatrices of coefficients corresponding to the correction vector Δ for the parameters of the aerial triangulation network; $L_{\delta_{X_i}}$, L_Δ are the constant terms vectors of the normal equations.

The matrix Q of inverse weights for the network parameters is determined from the equation:

$$\begin{bmatrix} C_{ii} & C_{i\Delta} \\ C_{i\Delta}^T & N_{\Delta\Delta} \end{bmatrix} \begin{bmatrix} Q_{ii} & Q_{i\Delta} \\ Q_{i\Delta}^T & Q_{\Delta\Delta} \end{bmatrix} = E, \quad (4)$$

where E is the identity matrix.

Solving equation (4) for Q_{ii} yields M_{X_i}—the covariance matrix of the errors for the coordinates of a ground point i:

$$M_{X_i} = \mu^2[C_{ii}^{-1} + C_{ii}^{-1}C_{i\Delta}(N_{\Delta\Delta} - C_{i\Delta}^T C_{ii}^{-1} C_{i\Delta})^{-1} C_{i\Delta}^T C_{ii}^{-1}], \quad (5)$$

where μ is RMS of unit weight for random errors of coordinate measurements on images.

The main diagonal of the matrix M_{X_i} contains the variances of the spatial coordinate errors for a terrain point i.

An algorithm for determining the accuracy of model point coordinates was implemented in our proprietary BlockMSG software [16, 17].

Results of point coordinate determination accuracy analysis

The image coordinates of points were obtained by computer vision modules in Agisoft Metashape software. As a result of automatic point recognition on the images, photogrammetric point coordinates (correspondences) were determined in the Agisoft software. These, along with adjustment parameters, served as the input data for processing in BlockMSG software [16, 17]. During the bundle adjustment computations, the RMS of the coordinate determination for each aerial triangulation point was calculated. In addition to this information, data on the number of images used to determine the coordinates of each point proved to be very valuable for the analysis.

The distribution of the number of images used to determine the coordinates of each object point for the two surveys in May 2025 and September 2025 are shown in **Figs. 4*a*** and **4*b***. As can be seen, this distribution does not correspond to the image overlap distribution shown in Fig. 2.

Histograms of point distribution by the number of images and the distribution of RMS errors in point coordinates for the two surveys from May 2025 and September 2025 are shown in **Figs. 5*a*** and **5*b***, respectively.

It can be seen in Fig. 5*a* that 42% of points are recognized in only two images, another 18% of points appear in three images, while from Fig. 5*b*, 54% of points are recognized in only two images, with another 18% appearing in three images.

There is a relationship between the number of images per point and RMS errors of coordinate determination, indicating that to determine the Z coordinate with an accuracy of 0.05 m (with a horizontal accuracy of 0.02–0.03 m), a minimum of 9 images of the point is required. Increasing the number of images from 407 to 870 reduced RMS errors of points determined from two and three images by approximately 30%. For the remaining points, the statistics remained virtually unchanged. If the distribution of RMS coordinate errors is plotted on a plane according to point coordinates, the resulting RMS error m_z surfaces are shown in **Figs. 6*a*** and **6*b*** for both surveys.

The RMS error surfaces m_x and m_y exhibit a similar spatial distribution to that of m_z, but are approximately two times smaller in magnitude.

Conclusions

The analysis of RMS distribution of coordinate determination over the object surface shows that areas with the highest RMS values exceeding 0.5 m correspond to water surfaces near the dam crest and pools of fluid at the dam base formed as a result of seepage processes. The most suitable areas for deformation determination are those with minimal determination errors ($m_z < 0.1$ m), which are associated with the most open, vegetation-free surfaces. The remainder of the dam surface is covered with grassy vegetation.

Furthermore, a correlation has been established between the number of images per point and RMS of point coordinate determination. This correlation indicates that to determine the Z coordinate with an accuracy of 0.05 m (and 0.02–0.03 m in plan view), a point must be visible in at least 9 images. However, despite this correlation, increasing the number of flight lines from 5 to 7 and the total number

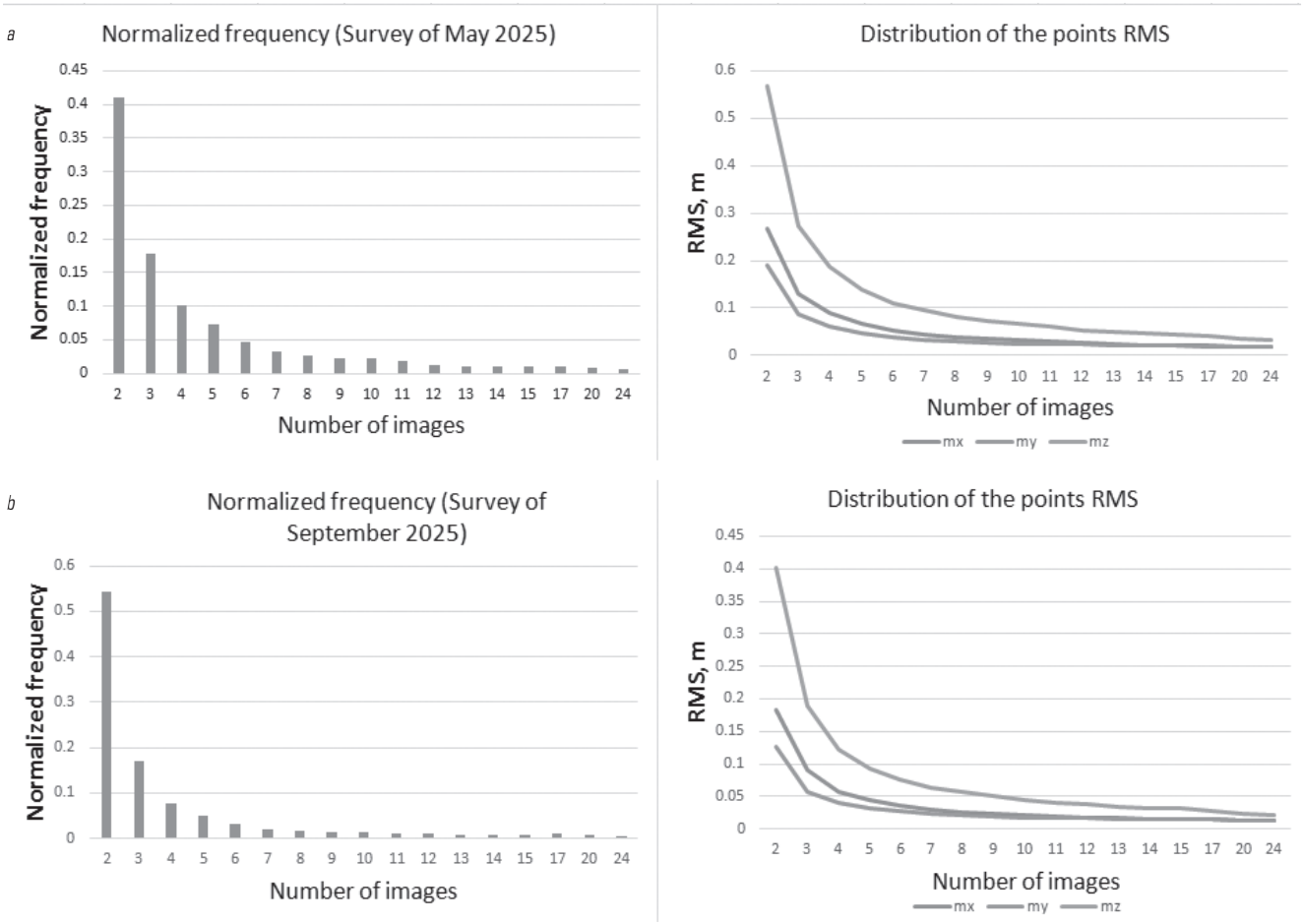

Fig. 5. Normalized frequency and distribution of RMS points:
a – Survey of May 2025 ; *b* – Survey of September 2025

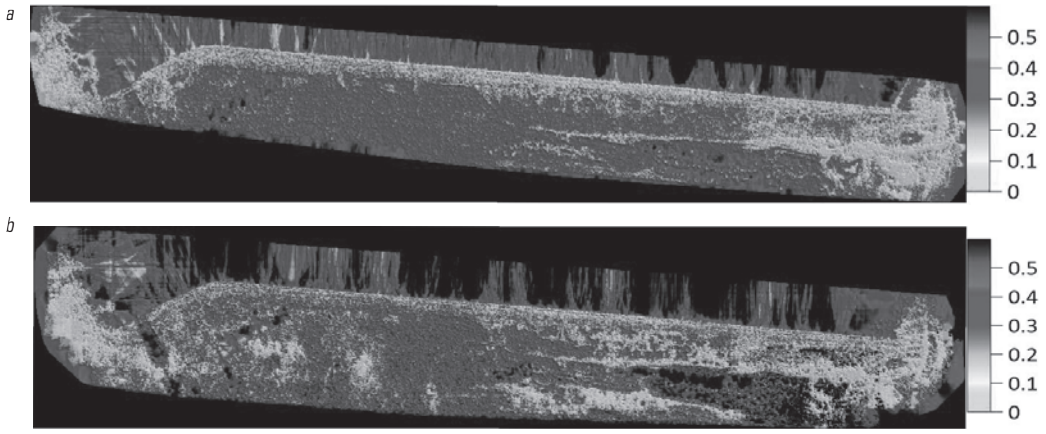

Fig. 6. Surface distribution of the RMS error mz, in meters:
a – Survey of May 2025; *b* – Survey of September 2025

of images from 407 to 870 did not lead to an increase in the number of images per point. This is due to two factors. First, when selecting identified points using computer vision methods, the intersection angles of the projecting rays are not taken into account (see Fig. 3). The second factor is related to image quality and spatial resolution. For reliable ground point recognition, GSD is required—no more than 2 cm/pixel. In the experimental surveys, it was 5.23 cm/pixel for the May 2025 survey and 3.19 cm/pixel for the September 2025 survey.

To improve the spatial resolution of the images, the flight altitude can be reduced.

Another factor influencing the subsequent recognition of points by computer vision algorithms is image quality. The aerial survey utilized a DJI M3E camera with a mechanical shutter. Compensating for the shutter shift during camera self-calibration also affects the recognition quality of the images. For camera self-calibration, it is necessary to have ground control points whose coordinates are determined with high accuracy and which are positioned to cover the entire area of the object. The coordinates of the photograph centers must be determined in post-processing mode from three base stations with an accuracy of less than 10 mm. If it is not possible to place ground control points on the object for self-calibration, then camera calibration must be performed on specialized calibration test fields [18].

To increase the number of images per point, it is recommended not to increase image overlap but to use a system of cross-flight lines and add flight lines with camera tilt.

Considering the existing experience in monitoring earth-fill dams [7, 18], it can be expected that the accuracy of determining point coordinates obtained from post-processing UAV photogrammetry data can be improved to 20 mm, thereby achieving the accuracy of LiDAR surveys. While this expected accuracy is not suitable for areal monitoring of rapidly developing processes, it can be a useful tool for geodetic monitoring, as it allows for seasonal control of the earth-fill dam body, ensuring the safe operation of such structures. Monitoring dams and embankments using photogrammetric methods does not exclude the application of other monitoring methods but rather complements them, enabling the identification of areas with anticipated deformations, the monitoring of which is recommended to be carried out using geodetic methods.

In addition, it is recommended to use UAV with thermal and multispectral cameras for monitoring embankment dams. This approach allows for the remote detection of areas with increased filtration and other parameters [19] necessary for the safe operation of the structure [20, 21].

Acknowledgements

The study was performed within the frameworks of agreement on grant financing for young scientists in scientific and scientific-technical projects of the Republic of Kazakhstan, Agreement No. 113/KMU-5-24-26 dd. 20.06.2024, project No. AP22788508.

References

1. RD 153-34.2-21.342-2001 Instructions for geotechnical monitoring of hydroelectric power station dams. Moscow : NIIAS, 2001. 24 p.
2. SP 47.13330.2016 Engineering Surveys for Construction. Basic Provisions. Available at: https://docs.cntd.ru/document/456045544 (accessed: 17.12.2025).
3. SP 39.13330.2012 Dams made of earth materials (SNiP 2.06.05-84). Available at: https://docs.cntd.ru/document/1200095521 (accessed: 17.12.2025).
4. Recommendations for conducting visual observations and surveys on earth dams. 2000. Available at: https://ohranatruda.ru/upload/iblock/070/4293812137.pdf (accessed: 15.12.2025).
5. Dam Surveillance Guide. Paris: International Commission on Large Dams. 2016. 109 p.
6. Ustinov A. V., Kaftan V. I. Technology of geodetic monitoring of hydropower structures during compensation grouting. *Power Technology and Engineering*. 2019. Vol. 53, No 2. pp. 129–134.
7. Sholomitsky A. A., Khannanov R. R., Tutanova M. S. Method of geodetic monitoring for bulk hydrotechnical structures. *Vestnik SGUGiT*. 2023. Vol. 23, No. 5. pp. 43–57.
8. Taddia Y., Stecchi F., Pellegrinelli A. Coastal mapping using DJI Phantom 4 RTK in post-processing kinematic mode. *Drones*. 2020. Vol. 4, Iss. 2. ID 9.
9. Kosarev N. S., Kolesnikov A. A., Reznik A. V., Nemova N. A., Ozhogin D. S. The use of geospatial data in the industrially disturbed land evaluation. *Journal of Mining Science*. 2023. Vol. 59, No. 6. pp. 1058–1065.
10. Ridolfi E., Buffi G., Venturi S., Manciola P. Accuracy analysis of a dam model from drone surveys. *Sensors*. 2017. Vol. 17, Iss. 8. ID 1777.
11. Buffi G., Manciola P., Grassi S., Barberini M., Gambi A. Survey of the Ridracoli Dam: UAV-based photogrammetry and traditional topographic techniques in the inspection of vertical structures. *Geomatics, Natural Hazards and Risk*. 2017. Vol. 8(2). pp. 1562–1579.
12. Pitombeira K., Mitishita E. Influence of on-site camera calibration with sub-block of images on the accuracy of spatial data obtained by PPK-based UAS photogrammetry. *Remote Sensing*. 2023. Vol. 15, No. 12. ID 3126.
13. James M. R., Robson S., d'Oleire-Oltmanns S., Niethammer U. Optimising UAV topographic surveys processed with structure-from-motion: Ground control quality, quantity and bundle adjustment. *Geomorphology*. 2017. Vol. 280. pp. 51–66.
14. Himmy O., Nguyen T. T., Vazhacharickal P. J., Buerkert A. Monitoring of granite quarries using deep learning and UAV photogrammetry in Bengaluru, India. *PLoS One*. 2025. Vol. 20, No. 11. ID e0334493.
15. Kazantseva V. V., Ozhigin D. S., Kosarev N. S., Satbergenova A. K., Ozhigina S. B. Development of complex system of geotechnical monitoring of technogenic objects based on geospatial data. *Journal of Mining Institute*. 2025. Vol. 276, Iss. 1. pp. 142–156.
16. Mogilny S. G. Programmauswahl der zusätzlichen Parametr bei der Bändelblockausglei-chung. *Bildmessung und Luftbildwesen*. 1981. Vol. 49. pp. 181–190
17. Company website of geosystems. Available at: https://vingeo.com/Rus/download.html (accessed: 17.12.2025).
18. Sholomitsky A. A, Akhmedov B. N, Ivanov A. V, Medvedskaya T. M. Accuracy of 3D photogrammetric bench coordinates determination. *Mine Surveying and Subsurface Use*. 2021. Vol. 2 (112). pp. 38–41.
19. de Mattos Teixeira C. A., Alves de Araujo T. M., Cardoso E., Costantin Filho M. A., Weyl Costa J. et al. Aerial image segmentation of embankment dams based on multispectral remote sensing: A case study in the Belo Monte Hydroelectric Complex, Pará, Brazil. *Peer J Computer* Science. 2025. Vol. 11. ID e2917.
20. Mussin R. A., Yachsishin M. G., Golik A. V., Akhmatnurov D. R. Block modeling reserves estimation. *Complex Use of Mineral Resources*. 2026. Vol. 339(4). pp. 97–103.
21. Bakhtybaev N., Mussin R., Alzhanov R., Zeitinova S., Abil O. Study of Potential Failure Points of Ventilation Shafts. *Journal of Studies in Science and Engineering*. 2025. Vol. 5(1). pp. 295–314. EM